Research article

An automatic optical inspection system for measuring a microlens array with an optical interferometric microscope and genetic algorithm

Shih-Wei Yang
Department of Electrical and Control Engineering, National Chiao Tung University, Hsinchu, Taiwan

Chern-Sheng Lin
Department of Automatic Control Engineering, Feng Chia University, Taichung, Taiwan

Shir-Kuan Lin
Department of Electrical and Control Engineering, National Chiao Tung University, Hsinchu, Taiwan

Shu-Hsien Fu
Department of Automatic Control Engineering, Feng Chia University, Taichung, Taiwan, and

Mau-Shiun Yeh
Chung-Shan Institute of Science and Technology, Lung-Tan, Taiwan

Abstract
Purpose – The purpose of this paper is to propose an automatic optical inspection system for measuring the surface profile of a microlens array.
Design/methodology/approach – The system set-up was constructed according to the principle of the Fizeau interferometer. After capturing the ring interference fringe images of the microlens with a camera, the diameter, profile information and optical properties were analyzed through a microlens surface profile algorithm using innovative image pre-processing with a precision of less than 0.09 micron.
Findings – By integrating with the genetic algorithm, the XY-Table shortest moving path of the system is calculated to achieve the purpose of high-speed inspection and automatic microlens array surface profile measurement.
Originality/value – The measurement results of this system were also compared with other systems, including the atomic force microscope and stylus profiler, to verify the measurement precision and accuracy of this system.

Keywords Inspection, Automation, Genetic algorithms, Surface properties of materials, Automatic optical inspection system, Microlens array, Surface profile

Paper type Research paper

1. Introduction

In recent years, microlens arrays have been widely used in a variety of applications. Single microlenses have been used to couple light to optical fibers, while microlens arrays are often used to increase the light collection efficiency (Lin *et al.*, 2010a). Industrial inspection of micro-devices is often a challenging task. As the lens becomes increasingly smaller in size, the inspection results will vary from person to person in the case of manual detection, and misjudgment may result from eye fatigue due to long working hours. Therefore, an automatic inspection system for measuring the surface profile of the microlens array is proposed in this paper, and the moving path of XY-table is optimized with the genetic algorithm (GA) to improve the inspection efficiency.

The surface profile can be generally obtained with an atomic force microscope (AFM), scanning electronic microscope (SEM), stylus profiler or optical interferometers. Each of these techniques has particular applications and advantages. Since a stylus profiler is a type of contact measurement method,

The current issue and full text archive of this journal is available at **www.emeraldinsight.com/0144-5154.htm**

Assembly Automation
33/1 (2013) 57–67

[DOI 10.1108/01445151311294720]

This work was sponsored by the National Science Council under grant no. NSC 99-2221-E-035 -081 and Chung-Shan Institute of Science & Technology under grant no. CSIST-757-V101.

it may easily damage the surface of the testing objects during inspection. Therefore, non-contact type interferometer like the proposed system based on Fizeau interferometer for optical inspection is more suitable for cases requiring high precision and relatively inexpensive requirements (Andreev *et al.*, 2005; Chen *et al.*, 2002; Teng and Lang, 2008). Microscope interferometry technology (Windecker *et al.*, 2001; Yamamoto and Yamaguchi, 2000) has been applied in optical inspection for a long period of time. The optical fringe projection method with phase shifting (Chen *et al.*, 2000; Pavageau *et al.*, 2004) is a device for measuring the three-dimensional profile and shape of an object using projected light patterns and a camera system. The Fourier transform method (FTM) is also a powerful method to translate two interferograms with different phase shifting to achieve reliable phase demodulation in the measurement of surface profile (Hu *et al.*, 2006).

Charriere *et al.* (2006) used digital holographic microscopy to describe the characteristics of a microlens, which allowed objects to be measured in a wide range of shapes as the vibration did not require isolation. However, the measurement structure for the surface shape of a microlens was incompatible with the measurement structure of the light characteristics of a microlens, and had to be measured by two instruments. Gdeisata *et al.* (2005) proposed a novel technique termed an iterative linear digital phase locked loop (DPLL) for fringe-pattern demodulation. Huang *et al.* (1999) proposed a novel digital fringe projection (DFP) technique for quantitative evaluation of corrosion. In this paper, the optimization of the XY-table movement is considered in particular and implemented through the GA, thus shortening the inspection time.

GAs have been successfully used in the design of complex systems (Katayama and Sakamoto, 2000; Baker and Ayechew, 2003). In a GA, a candidate solution is represented by a sequence of numbers known as chromosomes or strings. Each element (gene) in a string (chromosome) represents an operation (Salehi and Tavakkoli-Moghaddam, 2009). Lin *et al.* (2008) used the family competition GA to remove defective breeds on TFT-LCD. The GA has also been used to find the optimal target template in an automatic optical (AOI) system, and save memory space by recording the target template based on the sequence mode (Lin *et al.*, 2009). As there will be manufacturing process defects of some microlenses during the fabrication of a microlens array model, the GA can be used to plan and derive the XY-table shortest moving path regarding these inspection points when modifying the model. In addition, in the microlens array samples, thanks to different positions and uneven thermal expansion and contraction, some points will be selected in the factory for inspection in cases of specific areas prone to defects or too many microlens array inspection points. In such cases, it is also suitable to apply the GA to plan the inspection shortest moving path (Ahn and Ramakrishna, 2002; Hu *et al.*, 2004; Chatterjee *et al.*, 1996; Goldberg and Lingle, 1985) to shorten the system measurement time, and hence improving the system efficiency. Several optimization algorithms had been developed and implemented for searching optimal traveling paths, commonly referred to as traveling salesman problem (TSP) and the shortest path. It is suitable to form a computational evolution model with GA (Gen *et al.*, 1997; Kuo *et al.*, 2010).

In this paper, the process of evaluating the microlens array inspection shortest moving path with GAs and the surface profile of the microlens will be illustrated step by step in the following sections. And the measurement data of comparing with other systems including the AFM and stylus profiler will be shown to verify the precision and accuracy of the proposed system.

2. Methods of microlens array measurement systems

There are three parts in this section. The process of calculating the microlens array inspection shortest moving path with GAs is illustrated as the first part. Then, the image processing method of the interference fringe images segmentation of the microlens is applied in the second part. And the surface profile of the microlens will be calculated through the outer interpolation method in the final part.

2.1 The calculation of the microlens array inspection shortest moving path

When inspecting the microlens array, the XY-table moves vertically and horizontally under the control of the software program. The high-magnification CCD camera captures an image of each movement, then processes and analyzes the image to get the profile information of the inspected microlens. In this study, the GA was used to calculate the XY-table shortest moving path. Then the order of the microlenses under inspection was put out to control the XY-table accordingly.

Figure 1 shows the process of using the GA to calculate the XY-table shortest moving path in this study.

The process was divided into six parts as illustrated step by step below.

(a) Encoding of the path of the XY-table

In this study, the center of each microlens for inspection was set in the XY-table coordinate system. The point is regarded as a gene and numbered by an integer number (1-N). In this way, each microlens for inspection forms a sequence of positive integers, representing a moving path of the XY-table, namely, the so-called chromosome as shown in Table I. The total number of microlenses is the length of the chromosome (N). The first number represents the starting point and the last number is the final microlens for inspection. In this study, we assumed the initial population was the size of 100 randomly produced chromosomes. If the value is set too low, the evolution will be too slow to easily fall into a local optimal solution. Generally, the value is set depending on the nature of the problem and the experimental results.

(b) Design of the fitness function

The fitness function evaluates the quality of each chromosome. The fitness function is set as the reciprocal of the total inspection path length of the XY-table. The total inspection path length is equal to the sum of all the distance that the XY-table went through, calculated from the first lens which is inspected to the last lens which is inspected and then back to the start. But the fitness of a good gene is usually lager than the worse one, that is the reason why we take the reciprocal as the results here. It can be set by equation (1), by which the chromosome fitness can be calculated:

Figure 1 Flow chart of evaluating the shortest moving path of the XY-table with the genetic algorithm

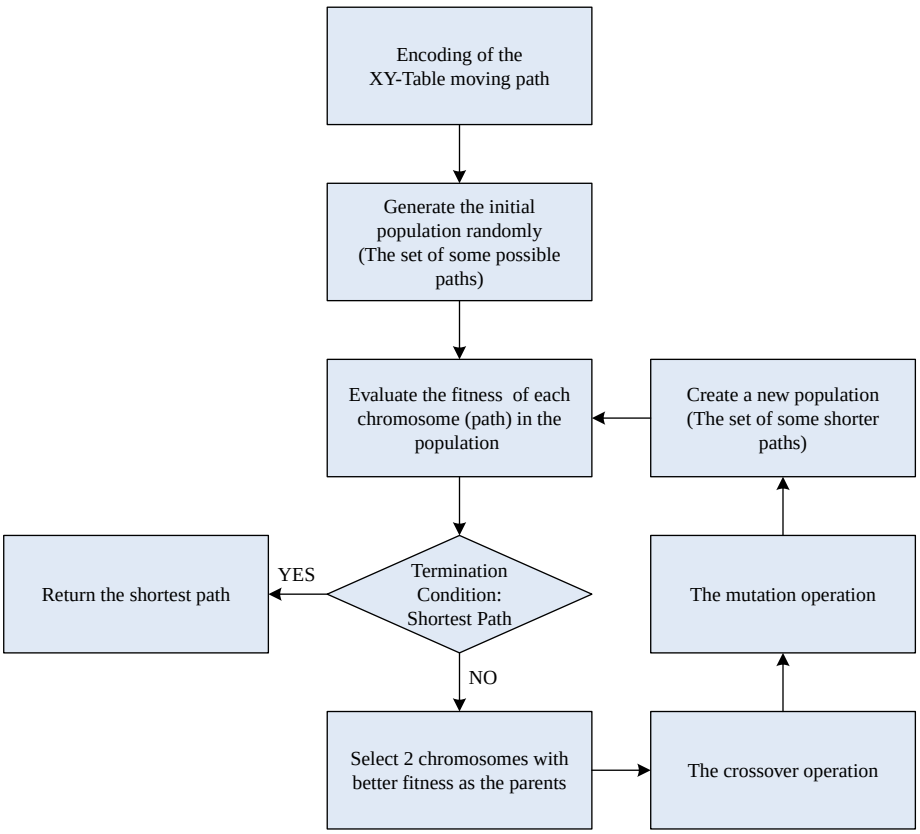

Table I XY-table path encoding

Chromosome	Inspection path sequence
Chromosome 1	1 2 3 4 5 6 7 ... (N − 2) (N − 1) N
Chromosome 2	7 9 11 21 18 5 4 ... (N − 1) 3 10
Chromosome 3	3 7 5 2 1 4 6 ... 14 (N − 2) N
⋮	
Chromosome 99	2 9 8 4 5 6 7 ... (N − 2) (N − 1) N
Chromosome 100	6 10 8 3 2 4 9 ... 5 17 N

$$D_{TOTAL} = \sum_{i=1}^{N-1} \left| \vec{V}_{ithLens} - \vec{V}_{(i+1)thLens} \right| + \left| \vec{V}_{NthLens} - \vec{V}_{1stLens} \right|$$

$$= \sum_{i=1}^{N-1} \sqrt{(x_{ithLens} - x_{(i+1)thLens})^2 + (y_{ithLens} - y_{(i+1)thLens})^2}$$

$$+ \sqrt{(x_{NthLens} - x_{1stLens})^2 + (y_{NthLens} - y_{1stLens})^2}$$

$$fitness = \frac{1}{D_{TOTAL}} \quad (1)$$

where:

D_{TOTAL} is the total path length.
$\vec{V}_{ithLens} = (x_{ithLens}, y_{ithLens})$ is the vector of No. i microlens corresponding to the starting point, and $(x_{ithLens}, y_{ithLens})$ are the coordinates.
N is 100 in this study.

This calculation aims to work out the shortest moving path. Hence, the corresponding fitness values of various chromosomes represent the reciprocal of the total path length of the system having completed the inspection and returned to the starting point. The larger the value is, the better it is as representing a shorter path.

As all normal physical equipments have some acceleration/deceleration (physical limitations) when they move, hence, for some special cases such as "the amount of the inspection points is close to the amount of all lenses", and "the total length of two paths is close", etc. the limits of the physical equipment and other factors should be considered when designing the fitness function. In this paper, the designed fitness function is simply for the cases described before.

(c) Selection

Selecting chromosomes of better fitness as the parent generation provides the expectation that the resulting offspring generations will also have better fitness. The method used in this study was the Roulette wheel selection, as shown in Figure 2(a). The Roulette wheel selection is based on the principle of better fitness occupying a larger area in the Roulette and thus having a higher chance of being selected, and the percentage is determined by all the path combinations according to fitness. Assume N darts are thrown out; N chromosomes are selected as the parental generation. If the hit chromosome is j, then the probability of selecting chromosome j P_j can be determined by equation (2):

Figure 2 (a) Diagram of the Roulette wheel selection method; (b) the partially-mapped crossover method; (c) the inversion mutation method

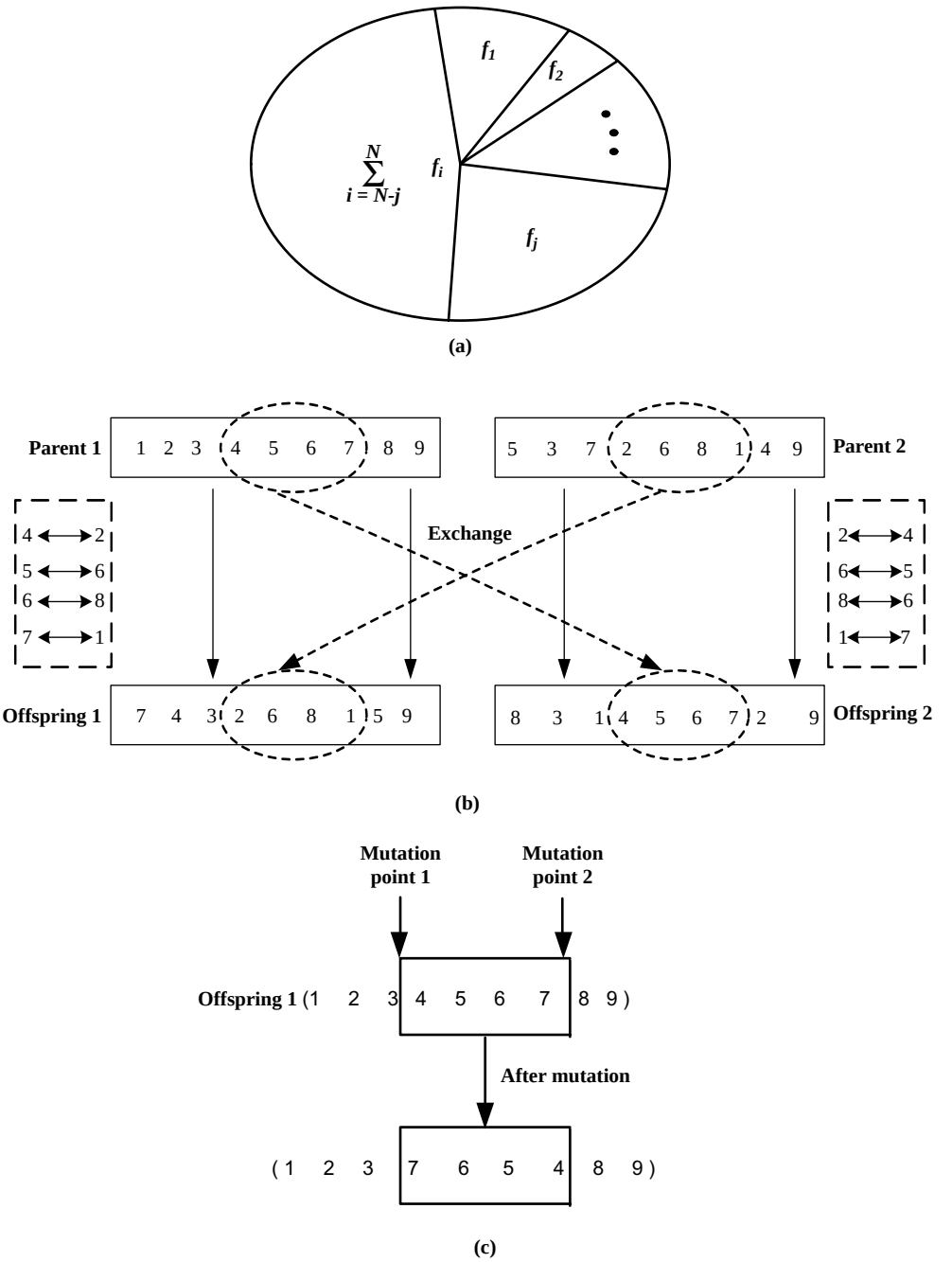

$$P_j = \frac{f_j}{\sum_{i=1}^{N} f_i} \quad (2)$$

where:

f_j is the fitness of chromosome j.
N is 100 in this study.

The selected parental generation is represented as the inspection path of the shorter total path length.

(d) Crossover

The selected parental generation of chromosomes is matched in pairs for crossover to produce the offspring generations, which are expected to produce a shorter inspection path. The crossover method used in this study was the partially-mapped crossover, which randomly selects two points as cutting points to divide the parental chromosome into the front, middle and later segments. The middle segment is crossed over first, while the genes of the front and later segments are filled in the original order, excluding the repeated ones (He and Hui, 2008). Figure 2(b) shows an example of the inspection path of nine microlenses.

Where (1 2 3 4 5 6 7 8 9) and (5 3 7 2 6 8 1 4 9) represent the inspection path of nine microlenses.

The new path produced by the crossover is not necessarily the shorter inspection path as compared with the parental generation. Hence, after each crossover calculation, the length of the new path must be calculated. If the new path is not shorter than the parental generation one, it will be rejected and the parental generation will be reproduced to the next stage population.

(e) Mutation
The occurrence of mutation keeps the path solution set from falling into the local optimal solution too easily. The mutation may lead to random changes of the inspection path, and new elements may be introduced into the solution set of all paths. However, mutation must not be too frequent; otherwise it may change the algorithm into a random algorithm. The mutation used in this study was the inversion mutation, which randomly selects two points in the inspection path sequence and changes inversely the sub-path between these two points. No path modification is needed after mutation. Figure 2(c) shows an example of the inspection path of nine microlenses.

(f) Termination condition
When the system calculates the XY-table shortest moving path of the inspection, the termination condition will be arrived at if the total path length is not shortened after 3,000 calculation cycles. Then, the inspection sequences of each microlens are put out on the shortest moving path. Each microlens will be inspected in such an order when using the XY-table.

2.2 Microlens array positioning
After capturing the image, the Newton's ring-shaped interference fringes of each microlens must be separated from the background, and each microlens should be positioned to facilitate the calculation of the grayscale change curve.

(a) Segmentation and noise removal
Interference fringes are often deep in color while the background is light colored, and the light filed uniformity differs from each other. The segmentation will not be suitable if using binarization of a single threshold value as it may result in numerous misjudgments. Considering the *R*-value is the dominant value of every pixel in the captured images. Hence, an novel mask operation is proposed to compare the *R*-value of the image pixel $R(x,y)$ with the mask average *R*-value $R_{avg}(x,y)$, to determine whether the pixel belongs to the background or the interference fringes, as shown in equation (3):

$$g'(x,y) = \begin{cases} 255 & if \;\; R(x,y) \geq R_{avg}(x,y) \\ 0 & else \;\; R(x,y) < R_{avg}(x,y) \end{cases} \qquad (3)$$

$$R_{avg}(x,y) = \frac{\sum_{i=1}^{n}\sum_{j=1}^{m} R(i,j)}{n \times m}$$

where:

- $g'(x,y)$ is the new gray value after the proposed mask operation, and $R(i,j)$ is the *R*-value of the pixel at coordinates (i,j) in the RGB color model.
- $R_{avg}(x,y)$ is the mask average *R*-value, and n, m is the size of the mask array.

After removing the background, the complete Newton's ring-shaped interference fringes and background binary image are shown as Figure 3.

(b) Newton's ring-shaped interference fringe segmentation
The interference fringe segmentation is performed to individually label each Newton's ring-shaped interference fringe. As each Newton's ring-shaped interference fringe is independent, the segmentation can be completed by the concept of connectivity.

(c) Center average of the individual interference fringe
After getting the Newton's ring-shaped interference fringes of each microlens, the center coordinates of the fringes can be averaged. The more accurate microlens array's center coordinates can be obtained.

(d) Microlens positioning
By extending from the lens center to the interference image background, the position, radius and profile of each microlens can be obtained correspondingly. The method extends from the lens center in four directions: 0°, −180°, 90°, −90°. The extensions in four directions are the right limit X_R, left limit X_L, upper limit Y_T, and lower limit Y_B. Using the coordinates of the four limit points (X_R, Y_T), (X_R, Y_B), (X_L, Y_B), (X_L, Y_T), each lens can be singled out and positioned.

2.3 Micro lens surface profile analysis
The grayscale curve of the interference image can be obtained along single microlens center. It is coded from left to right to obtain the brightness curve of the 1st segment, the 2nd segment, ..., and the *n*th segment. The phase angle of the interference fringes changes from 0° to 360°, indicating the microlens surface variation is λ/2. But the phase angles of the inner ring and outermost ring at the substrate are probably not a complete change.

Find maximum value T_i and minimum value D_i of the brightness curve of the *i*th segment, $g(x,y)$ is brightness of pixel (x,y) on the *i*th segment brightness curve.

Let Δ_i be the brightness variation of the *i*th segment when the phase angle changes from 0° to 180°, $\Delta_i = |T_i - D_i|$.

Let A_i be the brightness of the *i*th segment at a phase angle of 90°:

$$A_i = D_i + \frac{\Delta_i}{2}$$

The phase angle difference $\delta\theta(x, y)$ between the point (x, y) and $(x + 1, y)$ in the *i*th segment can be calculated as follows (Figure 4):

$$\delta\theta(x,y) = \cos^{-1}\left[2\frac{g(x,y) - A_i}{\Delta_i}\right] - \cos^{-1}\left[2\frac{g(x+1,y) - A_i}{\Delta_i}\right] \qquad (4)$$

where $g(x,y)$, $g(x + 1, y)$ are the gray level of the point (x, y) and $(x + 1, y)$. The phase angles α, β of the innermost and outermost rings of the interference fringe can be calculated by the outer interpolation method. Then the system can obtain microlens surface altitudes of respective pixels in segment.

Let the segment where center circle (x_c, y_c) lies be the nth segment, then the corresponding microlens surface altitude difference $\delta d(x)$ between point (x, y) and $(x + 1, y)$ in the *i*th segment can be obtained from the following equation (Lin *et al.*, 2010b):

Figure 3 Binary image of the circular interference fringes and the backgrounds

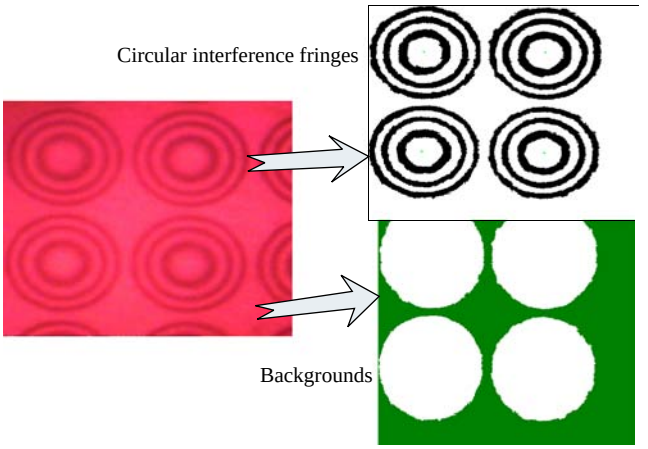

Figure 4 Grayscale curve and the parameters of the interference fringe phase angle change

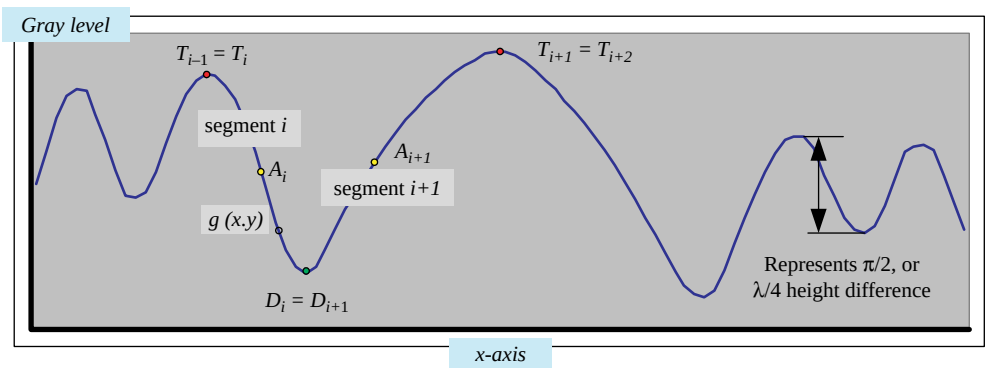

$$\delta d(x) = \left[\frac{\lambda}{4\pi}\right] \times \left|\cos^{-1}\left[2\frac{g(x,y) - A_i}{\Delta_i}\right] - \cos^{-1}\left[2\frac{g(x+1,y) - A_i}{\Delta_i}\right]\right| \quad (5)$$

Summation from the corresponding microlens surface altitude difference from a pixel in the 1st segment to the segment where the microlens center (x_c, y_c) lies (Figure 4), we can obtain lens sag (Δd):

$$\Delta d = \sum_{1}^{x_c} \delta d(x) \quad (6)$$

3. Experimental results and discussion

In this study, an AOI inspection system for the surface profile of a microlens array is proposed. A helium-neon red laser as the system light source and a high-magnification CCD camera in conjunction with a microscope set formed the image acquisition system. An optical plate was placed between the microscope and the microlens for inspection to get the interference fringe images of the microlens array. The XY-table controlled the movement of the microlens array in the x-axis and y-axis to capture the image of each microlens for inspection. Next, image processing was conducted and calculated to get the surface profile, diameter length, lens sag and other data through previous inference analysis. The diffuser of this structure was composed of a motor and a vibration film. Through the rotation of the diffuser, the noise generated by the laser was filtered. The structure was shown in Figure 5.

As shown in Figure 6(a), the microlens array was inspected using a 5×5 unit size. Regarding the 86×86 microlens samples used in this study, about 15×15 of a total of 225 sampling inspection points were selected to calculate the shortest moving path. As the inspection points were not regularly arranged, it would take many unnecessary paths and waste a lot of time if using the traditional column inspection method (path A in Figure 6(a)). Since there are probably not inspection points on some columns, the inspection time would be shortened if using the shortest moving path calculated in this study as the inspection path (path B in Figure 6(a)), and the shortest moving path can be derived from the following steps:

1 *Determining the starting point.* After selecting 225 sampling inspection points as shown in Figure 6(a), and no matter how these lenses distribute. The microlens which is nearest to the origin of the C++ graphic coordinate (upper left side) will be set as the starting point in the shortest path, and the corresponding coordinate is defined as $(\text{StartX}, \text{StartY})_{\text{XY-Table}}$. The XY-Table can be

Figure 5 Diagram and the physical set-up of the proposed inspection system design

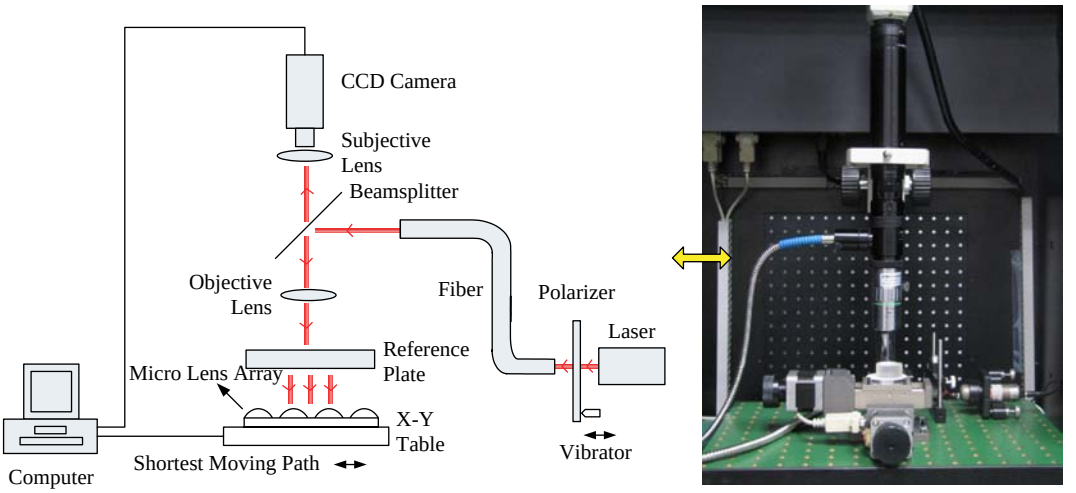

initialized by manual to the starting point, and (StartX, StartY)$_{\text{XY-Table}}$ will be equal to (0, 0)$_{\text{XY-Table}}$. If the XY-Table is moved to the starting point without initialization, then (StartX, StartY)$_{\text{XY-Table}}$ will be equal to a set of integers.

2 *Coordinate transformation.* Once the coordinate of the starting point is derived, every other microlens also has to be positioned for the XY-table. In other words, the coordinate of every microlens in the GA should be applied to the coordinate of XY-table, thus controlling the XY-table move according to the shortest path.

Defining the coordinate of the most upper left microlens in the microlens array is (1, 1), and the coordinates increase along the *x*-axis and *y*-axis form 1 to 86 as shown in Figure 6(b). Since the spacing between every microlens is 120 μm, and the unit step of XY-table is about 0.0 4μm, it takes 2,850 unit steps of XY-table to move from one microlens to another. Then, the coordinate transformation can be obtained from the following equations:

$$X_{XY-Table} = StartX_{XY-Table} + (X_{Sample} - 1) \times 2850 \quad (7)$$

$$Y_{XY-Table} = StartY_{XY-Table} + (Y_{Sample} - 1) \times 2850 \quad (8)$$

where, $X_{XY\text{-}Table}$ is the *x*-coordinate of the microlenses in XY-Table; $Y_{XY\text{-}Table}$ is the *y*-coordinate of the microlenses in XY-Table; X_{Sample} is the *x*-coordinate of the microlenses in the GA (the microlens array sample and the computer program); Y_{Sample} is the y coordinate of the microlenses in the GA (the microlens array sample and the computer program).

The coordinate of every microlens in the GA will be translated to the coordinate of XY-Table, thus controlling the XY-Table move according to the shortest path, as shown in Figure 6(c).

To simulate the conditions in the factory for inspection in cases of specific areas prone to defects or too many microlens array inspection points by the proposed system, four possible conditions including 100, 150, 200 and 225 inspection points are set up for experiments. According to the experimental results, it takes 2 s for the surface profile inspection of a single microlens, and 0.8 s for XY-Table moving from one microlens to another. For the above mentioned four experiments, the resulting data of each experiment is the average of five times as shown in Table II.

The specifications of the sample microlens array inspected in this study were provided by cooperative manufacturers. The diameter was 110 $\pm$ 0.5 μm, the curvature radius was 1.561 mm, and the array size was 10 mm $\times$ 10 mm $\times$ 1.2 mm. Moreover, the lens sag was verified to be 1.0 μm using mathematical equations and data provided by the manufacturers. Through the inspection system developed in this study, the lens sag of a single microlens can be obtained by using the above mentioned method to analyze the interference fringe images. The diameter length of a single microlens can be worked out using image processing and the conversion of each pixel against the real length.

To verify the accuracy of this system, we used the ET3000 surface profile measuring instrument developed by the KOSAKA Company and the atomic microscope (AFM) Dimension3100 developed by the Digital Instrument Company to inspect the lens sag and diameter length of the same sample microlens array (Figure 7(a) and (b)). The comparison of the measuring results of 80 microlenses is shown in Table III. Where, lens sag refers to the curve height of each lens of the microlens array as measured by the system, precision (standard deviation) refers to measuring of the same object in the same measuring procedure with the same data concentration, and accuracy refers to the difference between the average of numerous measurements and the actual value.

Figure 8 shows the accuracy and precision of the system. The accuracy value was below 0.04 μm and the precision value (standard deviation) was below 0.09 μm, showing the accuracy and precision of each lens were good.

The results suggested that the measuring results of this system were very close to the results of the other measuring equipment, with a gap below 2 percent. In addition, the microlens array surface might be damaged by the probe of the surface profile-measuring instrument, while the atomic microscope equipment is too expensive. The non-contact inspection method, low cost and high inspection speed of the proposed system proved its accuracy and usefulness.

Figure 6 (a) Traditional inspecting path A and the proposed shortest inspecting path B for the random sampled inspection; (b) the microlens coordinate system of the program; (c) the shortest inspecting path program interface

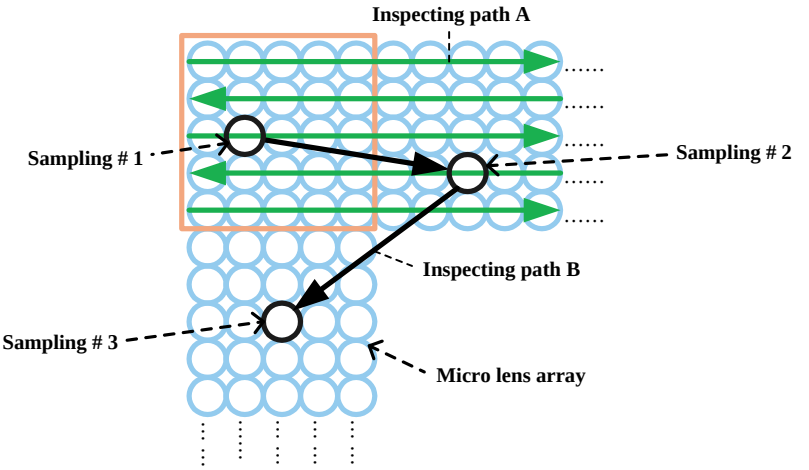

(a)

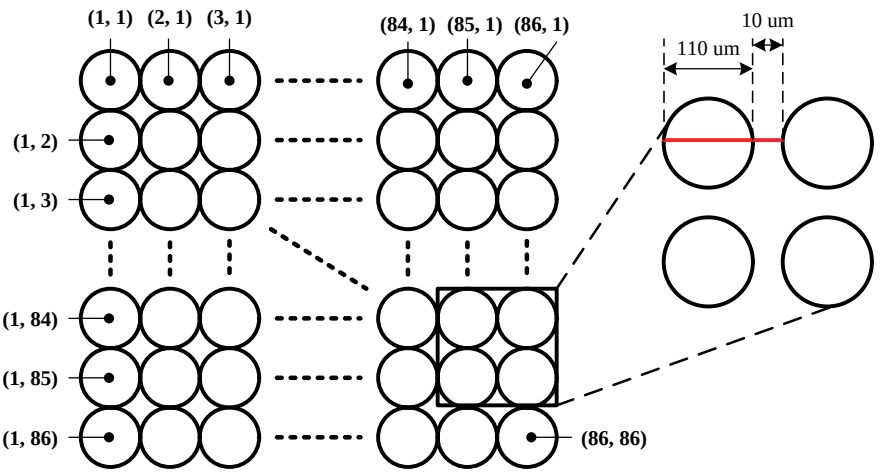

(b)

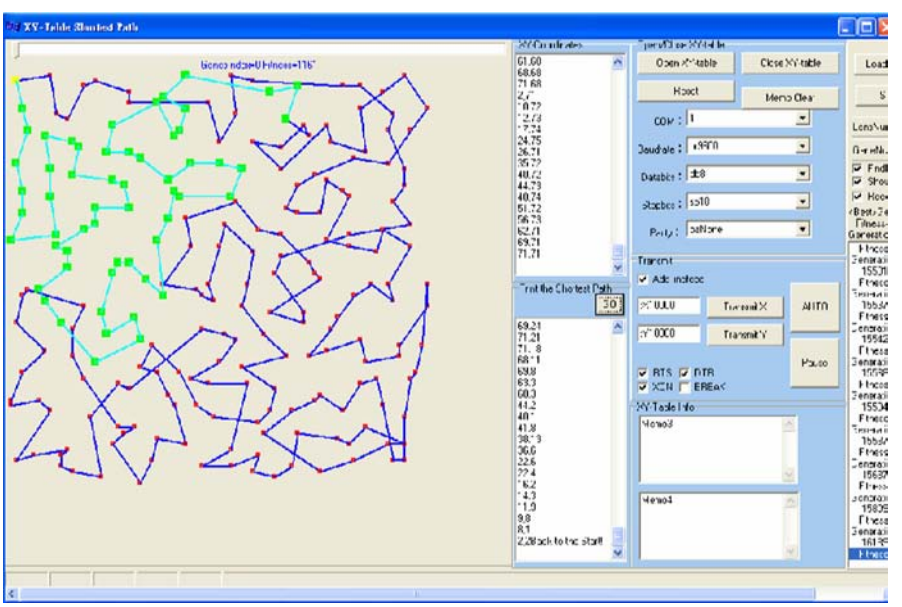

(c)

Table II Comparison of the time consumption of column scanning and the proposed method

Amount of microlenses	Unit size of sampling	Time consumption of column scanning (s)	Time consumption of shortest path (s)	Improving efficiency (%)
100	8 × 8 (10)	5,320	516.8	90.28
150	7 × 7 (12)	5,944.8	657.6	88.93
200	6 × 6 (14)	6,054.3	718.4	88.13
225	5 × 5 (15)	5,010.6	734.2	85.34

Figure 7 Measurement of the microlens array with different methods

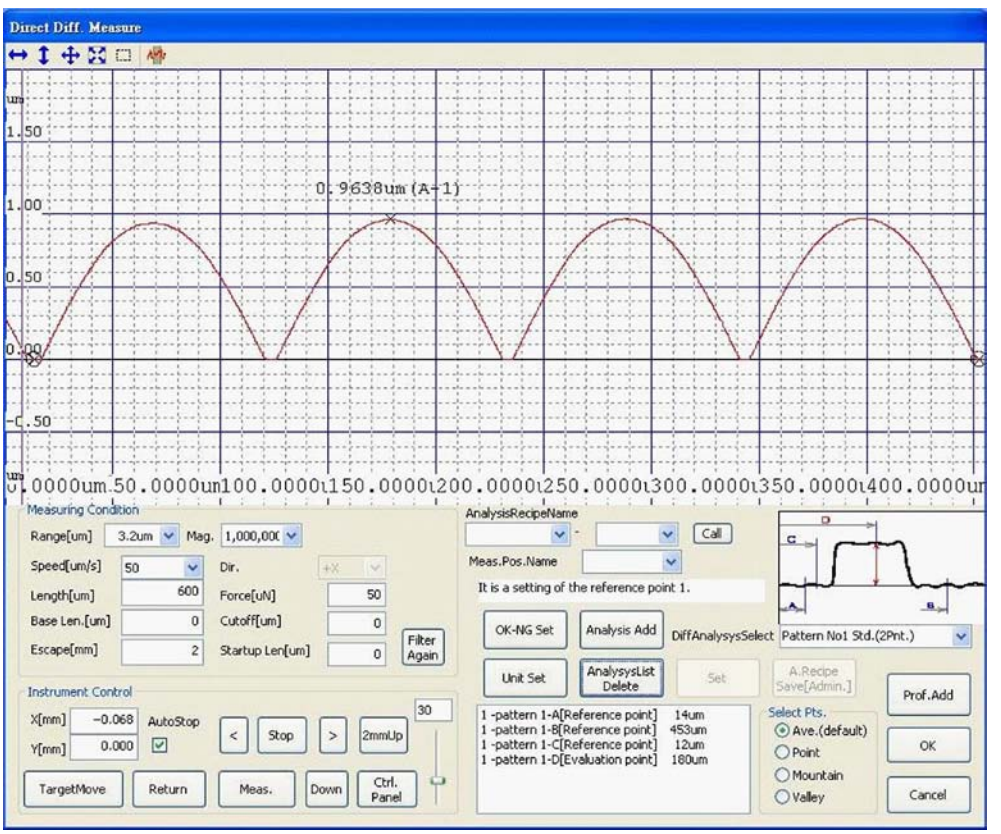

(a)

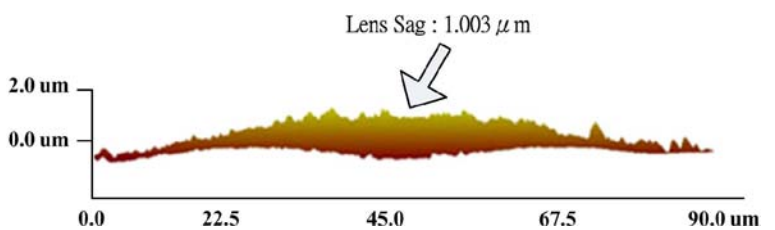

(b)

Notes: (a) Measurement results of the surface profilometer (KOSAKA,ET-3000); (b) measurement results of the scanning force microscopy (digital instrument, dimension 3100)

Table III Comparison of measuring results by this system, surface profile measuring instruments and the atomic microscope

Inspection item	This system	ET3000	Dimension3100AFM
Lens sag (μm)	0.96-1.01	0.95-0.99	1.003083
Diameter length (μm)	105-111	110-117	105-115

Figure 8 (a) Experimental results of lens sag measurements; (b) experimental results of precision and accuracy measurements

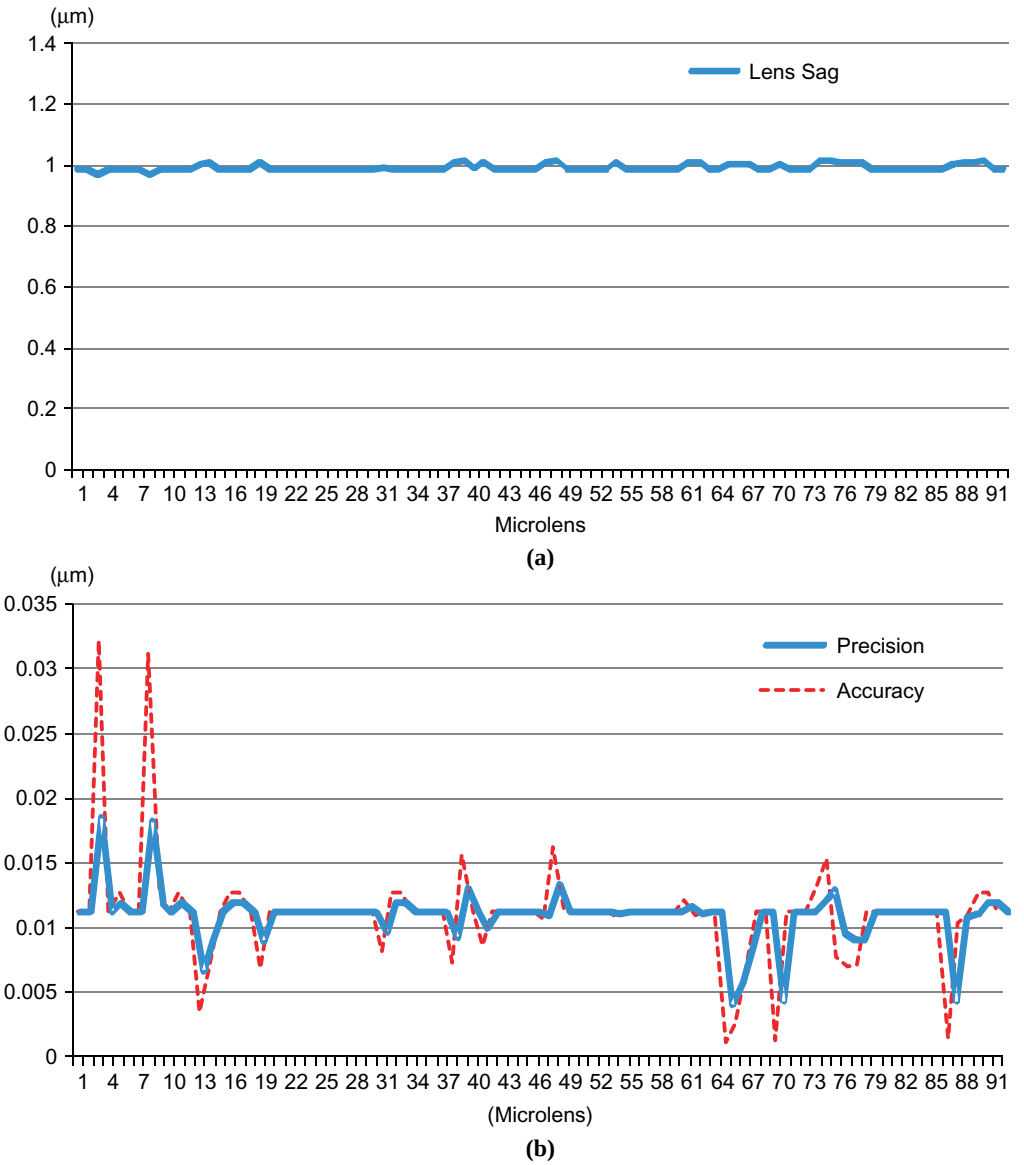

4. Conclusions

An AOI inspection system for the surface profile of a microlens array with an optical interferometric microscope is proposed in this paper. An optical plate was placed between the microscope set and the microlens array for inspection to form the ring-shaped interference fringes by the spherical surface and the plate reflection lights. The Fizeau interferometer principle is used to obtain the lens interferogram, and the GA is employed to calculate the shortest moving path of the XY-table, which is an innovative application for industry fields. The proposed system is simple structured, low cost, and specifically designed for the real time measurement according to the rapid inspection speed, and it has no need to coat a reflection layer on the microlenses, thus avoiding damaging the surface structure of the microlens sample.

References

Ahn, C.W. and Ramakrishna, R.S. (2002), "A genetic algorithm for shortest path routing problem and the size of populations", *IEEE Transactions on Evolutionary Computation*, Vol. 6 No. 6, pp. 566-79.

Andreev, V.A., Indukaev, K.V. and Ioselev, O.K. (2005), "Phase modulation microscopy MIM-2.1 for measurements of surface microrelief. Results of measurements", *J. Russ. Laser Res.*, Vol. 26 No. 5, pp. 394-401.

Baker, B.M. and Ayechew, M.A. (2003), "A genetic algorithm for the vehicle routing problem", *Computers & Operations Research*, Vol. 30, pp. 787-800.

Charriere, F., Kuhn, J., Colomb, T., Montfort, F., Cuche, E. and Emery, Y. (2006), "Characterization of microlenses by digital holographic microscopy", *Applied Optics*, Vol. 45 No. 5, pp. 829-35.

Chatterjee, S., Carrera, C. and Lynch, L.A. (1996), "Genetic algorithms and traveling salesman problems", *European Journal of Operational Research*, Vol. 93, pp. 490-510.

Chen, F., Brown, G.M. and Song, M. (2000), "Overview of three-dimensional shape measurement using optical methods", *Optical Engineering*, Vol. 39, pp. 10-22.

Chen, X., Grattan, K.T.V. and Dooley, R.L. (2002), "Optically interferometric roughness measurements for spherical surfaces by processing two microscopic interferograms", *Measurement*, Vol. 32, pp. 109-15.

Gdeisata, M.A., Burtonb, D.R. and Lalorb, M.J. (2005), "Fringe-pattern demodulation using an iterative linear digital phase locked loop algorithm", *Optics and Lasers in Engineering*, Vol. 43, pp. 767-75.

Gen, M., Cheng, R. and Wang, D. (1997), "Genetic algorithm for solving shortest path problems", *Proceedings of 1997 IEEE International Conference on Evolutionary Computing*, pp. 401-6.

Goldberg, D.E. and Lingle, R. (1985), "Alleles, loci, and the traveling salesman problem", *Proceedings of the First International Conference on Genetic Algorithms*, pp. 154-9.

He, Y. and Hui, C.W. (2008), "A rule-based genetic algorithm for the scheduling of single-stage multi-product batch plants with parallel units", *Computers & Chemical Engineering*, Vol. 32, pp. 3067-83.

Hu, X., Liu, G., Hu, C., Guo, T. and Hu, X. (2006), "Characterization of static and dynamic microstructures by microscopic interferometry based on a Fourier transform method", *Meas. Sci. Technol.*, Vol. 17, pp. 1312-18.

Hu, X.B., Wu, S.F. and Jiang, J. (2004), "On-line free-flight path optimization based on improved genetic algorithms", *Engineering Applications of Artificial Intelligence*, Vol. 17 No. 8, pp. 897-907.

Huang, P.S., Jin, F. and Chiang, F.P. (1999), "Quantitative evaluation of corrosion by a digital fringe projection technique", *Optics and Lasers in Engineering*, Vol. 31, pp. 371-80.

Katayama, K. and Sakamoto, H. (2000), "The efficiency of hybrid mutation genetic algorithm for the travelling salesman problem", *Mathematical and Computer Modelling*, Vol. 31, pp. 197-203.

Kuo, I.H., Horng, S.J., Kao, T.W., Lin, T.L., Lee, C.L., Chen, Y.H., Pan, Y. and Terano, T. (2010), "A hybrid swarm intelligence algorithm for the travelling salesman problem", *Expert Systems*, Vol. 27 No. 3, pp. 166-79.

Lin, C.S., Ho, C.W., Yang, S.W., Chen, D.C. and Yeh, M.S. (2010a), "Automatic optical inspection system for the image quality of microlens array", *Indian Journal of Pure and Applied Physics*, Vol. 48 No. 9, pp. 635-43.

Lin, C.S., Liao, Y.C., Lay, Y.L., Lee, K.C. and Yeh, M.S. (2008), "High-speed TFT LCD defect detection system with genetic algorithm", *Assembly Automation*, Vol. 28 No. 1, pp. 69-76.

Lin, C.S., Wu, K.C., Lay, Y.L., Lin, C.C. and Lin, J.M. (2009), "An automatic template generating method of machine vision system in TFT LCD assembly and positioning process with genetic algorithm", *Assembly Automation*, Vol. 29 No. 1, pp. 41-8.

Lin, C.S., Loh, G.H., Fu, S.H., Yang, S.W., Chang, H.K. and Yeh, M.H. (2010b), "An automatic evaluation method for the surface profile of the microlens array using an optical interferometric microscope", *Meas. Sci. Technol.*, Vol. 21 No. 11, pp. 1-10.

Pavageau, S., Dallier, R., Servagent, N. and Bosch, T. (2004), "A new algorithm for large surfaces profiling by fringe projection", *Sensors and Actuators A*, Vol. 115, pp. 178-84.

Salehi, M. and Tavakkoli-Moghaddam, R. (2009), "Application of genetic algorithm to computer-aided process planning in preliminary and detailed planning", *Engineering Applications of Artificial Intelligence*, Vol. 22 No. 8, pp. 1179-87.

Teng, H.K. and Lang, K.C. (2008), "Polarization shifting interferometric profilometer", *Optics and Lasers in Engineering*, Vol. 46, pp. 203-10.

Windecker, R., Fleischer, M., Korner, K. and Tiziani, H.J. (2001), "Testing micro devices with fringe projection and white light interferometry", *Optics and Lasers in Engineering*, Vol. 36, pp. 141-54.

Yamamoto, A. and Yamaguchi, I. (2000), "Surface profilometry by wavelength scanning Fizeau interferometer", *Optics and Laser Technology*, Vol. 32, pp. 261-6.

Corresponding author

Chern Sheng Lin can be contacted at: lincs@fcu.edu.tw